Supplemental Material for: Covalency-driven collapse of strong spin-orbit coupling in face-sharing iridium octahedra

Mai Ye,[1,*] Heung-Sik Kim,[1,†] Jae-Wook Kim,[1] Choong-Jae Won,[2,3] Kristjan Haule,[1] David Vanderbilt,[1] Sang-Wook Cheong,[1,4] and G. Blumberg[1,5,‡]

[1]*Department of Physics and Astronomy, Rutgers University, Piscataway, NJ 08854, USA*
[2]*Max Planck POSTECH/Korea Research Initiative, Pohang University of Science and Technology, Pohang 37673, Korea*
[3]*Laboratory of Pohang Emergent Materials, Pohang Accelerator Laboratory, Pohang 37673, Korea*
[4]*Rutgers Center for Emergent Materials, Rutgers University, Piscataway, NJ 08854, USA*
[5]*National Institute of Chemical Physics and Biophysics, 12618 Tallinn, Estonia*

Computational details

Ab-initio simulations

For our *ab-initio* simulations, we first assume a crystal structure with no disorder in Cu positions, that Cu are located at one of the three equivalent prismatic facial positions as shown in Fig. 2 in the main text. Further, no Cu-Ir intermixing is considered. The unit cell contains 6 formula units, i.e. three Ir-Cu chains. It should be commented that, for a better reproduction of the experimentally measured spectra one may need to take an average over *ab-initio* calculations from all possible orderings of Cu to restore the three-fold rotation symmetry along the chain direction. For a qualitative understanding of the high-energy spectra, however, the current result from the choice of Cu ordering shown in Fig. 2 in the main text seems to be enough.

The Vienna *ab-initio* Simulation Package (VASP), which uses the projector-augmented wave (PAW) basis set [1, 2], is employed for structural optimizations and electronic structure calculations. 400 eV and a Γ-centered 3x3x3 k-point grid are used for the plane wave energy cutoff and the k-point sampling, respectively. A revised Perdew-Burke-Ernzerhof generalized gradient approximation for crystalline solids (PBEsol) is chosen for the exchange-correlation functional [3], and 10^{-2} eV/Å of force criterion was used for the structural optimization. A simplified rotationally-invariant form of DFT+U method [4] is employed to treat the on-site Coulomb interaction both at Cu and Ir sites with the spin-orbit coupling (SOC) included.

Tight-binding model

Assuming the three-fold rotational symmetry along the chain direction (*i.e.* ignoring the IrO_6 octahedral distortions other than the trigonal one), and also assuming the Ir-Ir hybridizations are dominating those from Ir-Cu (this choice is justified by DFT calculations which show small hybridization between Ir and Cu d-orbitals), the three-site tight-binding model can be written as follows,

$$H_{\mathrm{TB}} = \left(\begin{array}{ccc|ccc|ccc} 0 & \Delta_{\mathrm{tri}} & \Delta_{\mathrm{tri}} & t_1 & t_2 & t_2 & 0 & 0 & 0 \\ \Delta_{\mathrm{tri}} & 0 & \Delta_{\mathrm{tri}} & t_2 & t_1 & t_2 & 0 & 0 & 0 \\ \Delta_{\mathrm{tri}} & \Delta_{\mathrm{tri}} & 0 & t_2 & t_2 & t_1 & 0 & 0 & 0 \\ \hline t_1 & t_2 & t_2 & \epsilon_{\mathrm{on}} & \Delta_{\mathrm{tri}} & \Delta_{\mathrm{tri}} & t_1 & t_2 & t_2 \\ t_2 & t_1 & t_2 & \Delta_{\mathrm{tri}} & \epsilon_{\mathrm{on}} & \Delta_{\mathrm{tri}} & t_2 & t_1 & t_2 \\ t_2 & t_2 & t_1 & \Delta_{\mathrm{tri}} & \Delta_{\mathrm{tri}} & \epsilon_{\mathrm{on}} & t_2 & t_2 & t_1 \\ \hline 0 & 0 & 0 & t_1 & t_2 & t_2 & 0 & \Delta_{\mathrm{tri}} & \Delta_{\mathrm{tri}} \\ 0 & 0 & 0 & t_2 & t_1 & t_2 & \Delta_{\mathrm{tri}} & 0 & \Delta_{\mathrm{tri}} \\ 0 & 0 & 0 & t_2 & t_2 & t_1 & \Delta_{\mathrm{tri}} & \Delta_{\mathrm{tri}} & 0 \end{array}\right),$$

where t_1 and t_2 are nearest-neighbor hopping integrals between the same and different kinds of Ir t_{2g} orbitals respectively, Δ_{tri} is the on-site trigonal crystal field within the t_{2g} complexes, and ϵ_{on} is the on-site energy difference between the central and lateral Ir. The projected density of states in Fig. 3(b) in the main text are calculated by choosing t_1 = -0.43 eV, t_2 = -0.20 eV, Δ_{tri} = -0.12 eV, and ϵ_{on} = -0.3 eV, which yield qualitative agreement with the *ab-initio* results as discussed in the main text. Note that, if we take the unitary transform to the trigonal basis set (a_{1g} and e'_g states), the σ-like overlap between the a_{1g} states becomes $t_1 + 2t_2$ = -0.83 eV, twice larger than the SOC of Ir ($\lambda_{\mathrm{SO}} \simeq 0.4$ eV), supporting the molecular-orbital scenario.

U_{Ir} dependence of the electronic structure

In the computations of projected DOS presented in the main text, the collinear magnetic configuration illustrated in Fig. S1(a) is employed. Note that in our calculations with various trial magnetic configurations, the Ir spin moments on an Ir trimer show a collective motion and favor the direction parallel to the Cu-Ir chain, consistent with the effect of MO formation and the role SOC discussed in the main text. Also note that the one depicted in Fig. S1(a) is the ground state configuration for our choice of Cu-Ir chain structure [see Fig. 1 in the main text], while the energetics and the ground state configuration may depend on a different choice of Cu order.

In our DFT+U calculations we choose the U value for Cu (denoted as U_{Cu}) to be 4∼6 eV. With this choice of U_{Cu} the

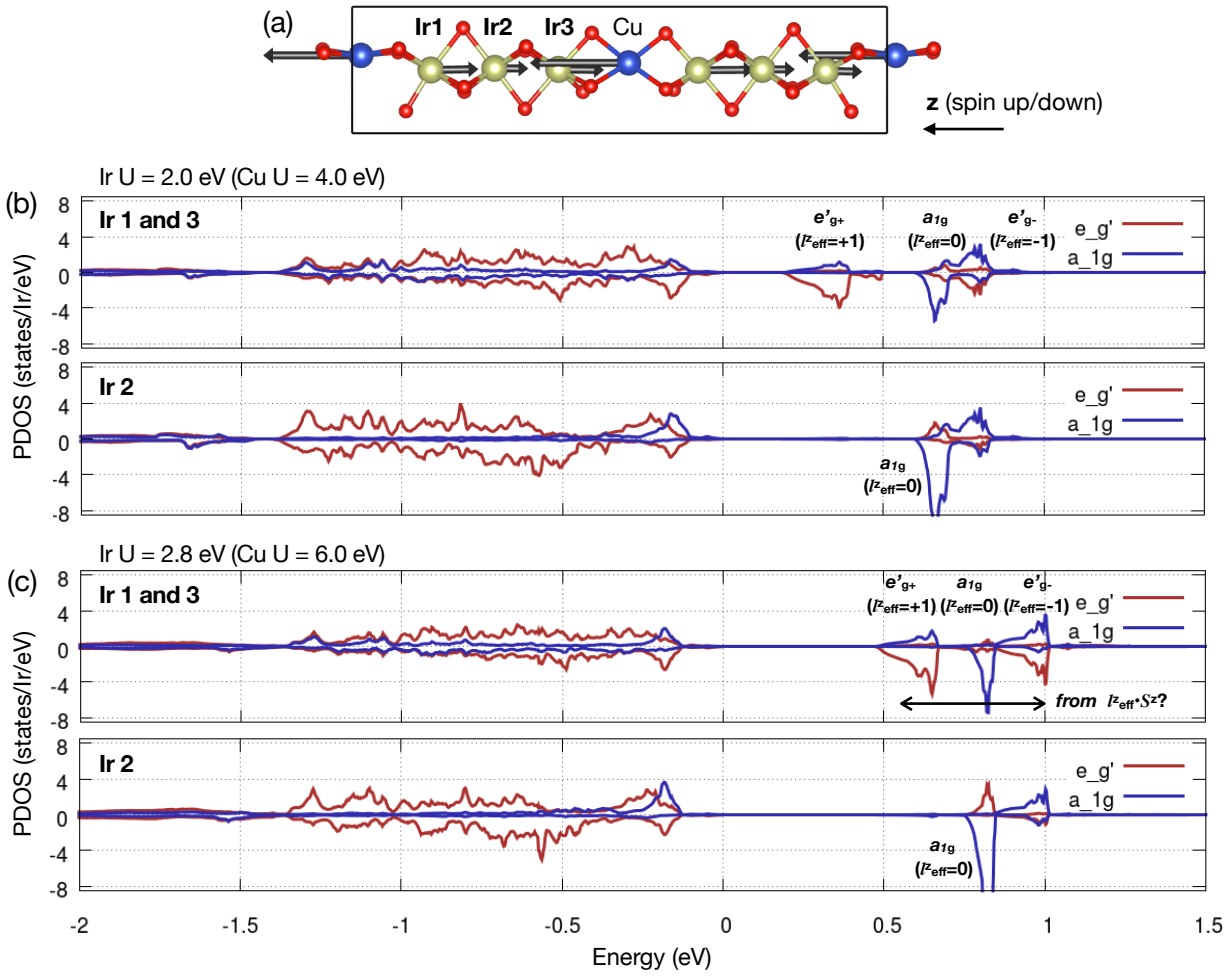

FIG. S1. (a) The ground state magnetic configuration in a Cu-Ir chain, where the black arrows depict the size and direction of the spin moments at Cu and Ir sites. (b,c) a_{1g}/e'_g-projected DOS with (b) $(U_{\rm Ir}, U_{\rm Cu})$ = (2, 4)eV and (c) (2.8, 6)eV.

Cu e_g orbital character is almost absent near the Fermi level, so that the electronic structure near the Fermi level is mostly determined by the Ir t_{2g} states. As discussed in the main text, the combination of Ir SOC and $U_{\rm Ir}$ induces the three-peak structure as observed in the Raman measurement. In the main text we employ $U_{\rm Ir}$ = 2.8 eV, and the three peak structure does not qualitatively change in the range of $2 < U_{\rm Ir} < 3$ eV. Fig. S1(b) and (c) show the projected DOS with $(U_{\rm Ir}, U_{\rm Cu})$ = (2, 4)eV and (2.8, 6)eV respectively. It can be seen that a smaller value of $U_{\rm Ir}$ induces a smaller charge gap, but the three-peak structure remains almost unchanged. The spacing between the three peaks in the upper Hubbard bands can be affected in a quantitative way with a different choice of $U_{\rm Ir}$.

Experimental details

Material preparation

Single crystals of $Ba_5CuIr_3O_{12}$ are grown by flux method; details of growth and characterization will be published separately. This material has a trigonal structure (space group $P3c1$, No.158; point group C_{3v}) [5, 6]. The sample is polished with a lapping film (1 micrometer, Buehler) and is subsequently annealed at 650 °C in air to remove residual strain. Its annealed (001) crystallographic surface is then used for Raman measurements.

Raman scattering

Raman-scattering measurements are performed in a quasi-back-scattering optical setup. The 476.2 nm line from a Kr^+ ion laser is for excitation. Incident light with ∼10 mW power is focused to a $50\times100\ \mu m^2$ spot on the (001) crystallographic surface. Environmental temperature of 20 K is achieved in a helium-gas-cooled cryostat, and the laser heating is assumed to be 0.5 K/ mW. We use a custom triple-grating spectrometer and a liquid-nitrogen-cooled charge-coupled device (CCD) detector for collection and analysis of the scattered light. The data are corrected for the system background and the spectral response. The measured scattering inten-

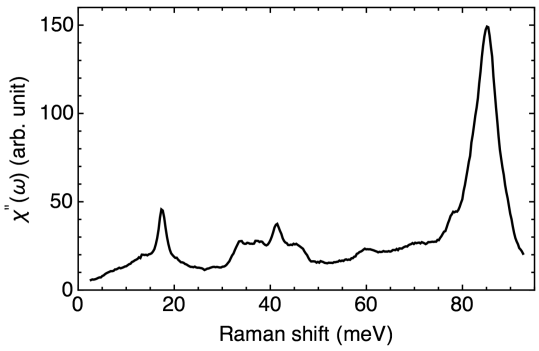

FIG. S2. Raman response $\chi''(\omega)$ of $Ba_5CuIr_3O_{12}$ at 25 K.

sity $I(\omega, T)$ is related to the Raman response $\chi''(\omega, T)$ by $I(\omega, T) = [1 + n(\omega, T)]\chi''(\omega, T)$, where n is the Bose factor, ω is Raman shift and T is temperature.

Low-energy Raman spectrum

Fig. S2 shows the low-energy Raman spectrum of $Ba_5CuIr_3O_{12}$ at 25 K. The sharp features at 17, 41 and 84 meV are identified as phonon modes. The 17 meV mode primarily involves motion of Ir atoms, and the 84 meV mode is derived from vibration of O atoms. The broad feature centered at 40 meV could be a bundle of phonon modes related to the motion of Ba atoms. The two weak features at 60 and 78 meV are also likely phonon modes.

* mye@physics.rutgers.edu
† hk676@physics.rutgers.edu
‡ girsh@physics.rutgers.edu

[1] G. Kresse and J. Furthmüller, "Efficient iterative schemes for ab initio total-energy calculations using a plane-wave basis set," Phys. Rev. B **54**, 11169–11186 (1996).
[2] G. Kresse and D. Joubert, "From ultrasoft pseudopotentials to the projector augmented-wave method," Phys. Rev. B **59**, 1758–1775 (1999).
[3] John P. Perdew, Adrienn Ruzsinszky, Gábor I. Csonka, Oleg A. Vydrov, Gustavo E. Scuseria, Lucian A. Constantin, Xiaolan Zhou, and Kieron Burke, "Restoring the density-gradient expansion for exchange in solids and surfaces," Phys. Rev. Lett. **100**, 136406 (2008).
[4] S. L. Dudarev, G. A. Botton, S. Y. Savrasov, C. J. Humphreys, and A. P. Sutton, "Electron-energy-loss spectra and the structural stability of nickel oxide: An LSDA+U study," Phys. Rev. B **57**, 1505–1509 (1998).
[5] Graeme R. Blake, Jeremy Sloan, Jaap F. Vente, and Peter D. Battle, "Prediction and Verification of the Structural Chemistry of New One-Dimensional Barium/Copper/Iridium Oxides," Chem. Mat. **10**, 3536–3547 (1998).
[6] Graeme R. Blake, Peter D. Battle, Jeremy Sloan, Jaap F. Vente, Jacques Darriet, and Franois Weill, "Neutron Diffraction Study of the Structures of $Ba_5CuIr_3O_{12}$ and $Ba_{16}Cu_3Ir_{10}O_{39}$," Chem. Mat. **11**, 1551–1558 (1999).